

# E2 interaction and dimerization in the crystal structure of TRAF6

Qian Yin<sup>1,2</sup>, Su-Chang Lin<sup>1</sup>, Betty Lamothe<sup>3</sup>, Miao Lu<sup>1</sup>, Yu-Chih Lo<sup>1</sup>, Gregory Hura<sup>4</sup>, Lixin Zheng<sup>5</sup>, Rebecca L Rich<sup>6</sup>, Alejandro D Campos<sup>3</sup>, David G Myszk<sup>6</sup>, Michael J Lenardo<sup>5</sup>, Bryant G Darnay<sup>3</sup> & Hao Wu<sup>1,2</sup>

**Tumor necrosis factor (TNF) receptor-associated factor (TRAF)-6 mediates Lys63-linked polyubiquitination for NF- $\kappa$ B activation via its N-terminal RING and zinc finger domains. Here we report the crystal structures of TRAF6 and its complex with the ubiquitin-conjugating enzyme (E2) Ubc13. The RING and zinc fingers of TRAF6 assume a rigid, elongated structure. Interaction of TRAF6 with Ubc13 involves direct contacts of the RING and the preceding residues, and the first zinc finger has a structural role. Unexpectedly, this region of TRAF6 is dimeric both in the crystal and in solution, different from the trimeric C-terminal TRAF domain. Structure-based mutagenesis reveals that TRAF6 dimerization is crucial for polyubiquitin synthesis and autoubiquitination. Fluorescence resonance energy transfer analysis shows that TRAF6 dimerization induces higher-order oligomerization of full-length TRAF6. The mismatch of dimeric and trimeric symmetry may provide a mode of infinite oligomerization that facilitates ligand-dependent signal transduction of many immune receptors.**

TRAFs have important roles in intracellular signal transduction of many receptor families such as the TNF receptor superfamily, the IL-1 receptors (IL-1R), the Toll-like receptors (TLR), T-cell receptors (TCR) and B-cell receptors (BCR)<sup>1,2</sup>. Upon receptor activation, TRAFs are directly or indirectly recruited to the intracellular domains of these receptors. They subsequently engage other signaling proteins to activate the inhibitor of  $\kappa$ B (I $\kappa$ B) kinase (IKK) and MAP kinases, leading ultimately to activation of transcription factors such as NF- $\kappa$ B and AP-1 to induce immune and inflammatory responses and confer protection from apoptosis.

Most TRAFs contain an N-terminal domain with a RING domain, a variable number of zinc fingers and a C-terminal TRAF domain that comprises a coiled coil domain and a conserved TRAF-C domain (Fig. 1a). Previous biochemical and structural studies have revealed that the TRAF domain forms a mushroom-shaped trimeric structure, with the TRAF-C domain as the head for interaction with receptors and adaptor proteins and the coiled coil domain as the stalk for trimerization<sup>3–5</sup>. Notably, TRAF6 is uniquely pleiotropic in participating in the signal transduction of many receptor systems, whereas TRAF2, TRAF3 and TRAF5 seem to signal only within the TNF receptor superfamily<sup>5</sup>.

The downstream signaling mechanism of TRAFs was first revealed from biochemical and cellular studies of TRAF6 to show the involvement of Lys63-linked polyubiquitination<sup>6–8</sup>. Ubiquitination is one of

the most prevalent post-translational modifications<sup>9</sup>. It is accomplished in three steps: (i) ATP-dependent attachment of ubiquitin via a thioester bond to a ubiquitin-activating enzyme (E1); (ii) transfer of ubiquitin from E1 to the active site cysteine of a ubiquitin-conjugating enzyme (E2); and (iii) transfer of ubiquitin from the E2 active site to lysine residues of substrates (including other molecules of ubiquitin) with the aid of a ubiquitin ligase (E3)<sup>10–12</sup>. There are two types of well-characterized E3s. The HECT domain-containing E3s harbor an essential catalytic cysteine residue and promote substrate polyubiquitination via an E3 intermediate with a thioester-linked ubiquitin. The RING domain-containing E3s do not seem to have catalytic activity but provide a bridge between E2s and substrates. TRAF6 is a RING-type E3 that facilitates Lys63-linked polyubiquitination. Unlike Lys48-linked polyubiquitin chains, which are hallmarks for proteasomal degradation, the Lys63 linkage is nondegradative and functions as a signaling moiety in DNA-damage repair processes and innate immunity pathways<sup>10,13</sup>.

Upon activation by the relevant signaling pathways after ligand stimulation, TRAF6 promotes Lys63-linked polyubiquitination of itself and downstream signaling proteins, a process that requires the heterodimeric E2 of Ubc13 and the ubiquitin E2 variant (Uev) known as Uev1A<sup>10</sup>. A crystal structure of the complex between Ubc13 covalently bound to donor ubiquitin and a Uev known as Mms2 has elegantly revealed that Uev possesses an acceptor ubiquitin binding site and

<sup>1</sup>Weill Medical College of Cornell University and <sup>2</sup>Tri-institutional Training Program in Chemical Biology, New York, New York, USA. <sup>3</sup>Department of Experimental Therapeutics, University of Texas M.D. Anderson Cancer Center, Houston, Texas, USA. <sup>4</sup>Advanced Light Source, Lawrence Berkeley National Laboratory, Berkeley, California, USA. <sup>5</sup>Laboratory of Immunology, National Institute of Allergy and Infectious Diseases, National Institutes of Health, Bethesda, Maryland, USA. <sup>6</sup>Center for Biomolecular Interaction Analysis, School of Medicine, University of Utah, Salt Lake City, Utah, USA. Correspondence should be addressed to H.W. (haowu@med.cornell.edu).

Received 13 November 2008; accepted 8 April 2009; published online 24 May 2009; doi:10.1038/nsmb.1605

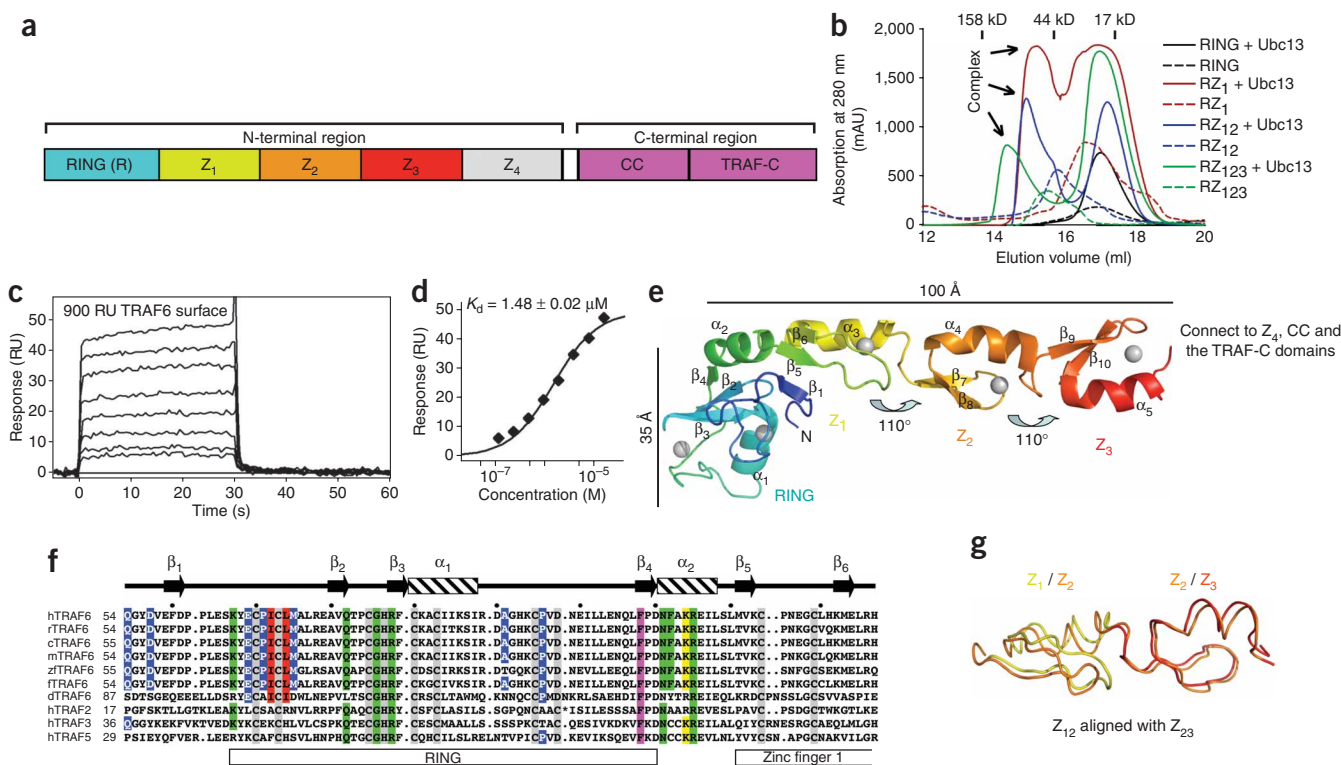


**Figure 1** Biochemical characterization of the TRAF6-Ubc13 interaction and structure of the N-terminal region of TRAF6. **(a)** Domain organization of TRAF6. Z<sub>1</sub>-Z<sub>4</sub>, zinc fingers 1-4; CC, coiled coil. **(b)** Superimposed gel filtration profiles of TRAF6-Ubc13 mixtures show that TRAF6 RZ<sub>1</sub> is both necessary and sufficient for Ubc13 interaction. Approximate elution positions of molecular weight standards are shown. **(c)** Surface plasmon resonance measurement for the binding of Ubc13 to surface-coupled TRAF6 RZ<sub>123</sub> at different Ubc13 concentrations. **(d)** Plot of the binding response as a function of Ubc13 concentration to derive the  $K_d \pm$  s.e.m. **(e)** Ribbon diagram of the monomer structure of TRAF6 RZ<sub>123</sub>. The different domains are labeled and the rotational relationships between the zinc fingers are shown. **(f)** Sequence alignment of TRAF6 from different species and with TRAF2, TRAF3 and TRAF5. Domain boundaries and secondary structures are labeled. Zinc-coordinating residues are shaded in gray. Residues at the Ubc13 interface are highlighted in red for those that bury more than 60 Å<sup>2</sup> in surface area and in blue for those with surface area burials of 20-60 Å<sup>2</sup>. Residues at the dimerization interface are highlighted in magenta for those that bury more than 100 Å<sup>2</sup> of surface area and in green for those with surface area burials of 40-100 Å<sup>2</sup>. The major TRAF6 autoubiquitination site at Lys124 is highlighted in yellow. \* in the TRAF2 sequence represents an insertion of 'VHEGIYEEG'. h, human; r, rat; c, cow; m, mouse; zf, zebra fish; f, fowl; d, *Drosophila*. **(g)** Superposition of the zinc finger 1 and 2 structure to the zinc finger 2 and 3 structure.

orientates the acceptor ubiquitin for Lys63 linkage with the donor ubiquitin<sup>14</sup>. The Lys63-linked polyubiquitin chains function as anchors to recruit the TAK1 kinase complex and IKK to activate both the MAP kinase pathway and the NF- $\kappa$ B pathway<sup>15</sup>. TAK1 directly phosphorylates MAP kinases, whereas IKK-mediated phosphorylation of I $\kappa$ B leads to its degradation to free NF- $\kappa$ B for transcription.

Despite extensive studies, how TRAF6 and other E3s promote polyubiquitination is poorly understood. Here we report biochemical, structural and cell biological studies on the N-terminal region of human TRAF6 that reveal both the specificity and mechanism of TRAF6-mediated polyubiquitination. We show that the RING domain of TRAF6 does not function alone; instead, residues preceding the RING directly interact with Ubc13, and the first zinc finger has a structural role. Unexpectedly, we show that the N-terminal region of TRAF6 is dimeric, in contrast to the trimeric symmetry of its C-terminal region. Investigation of the functional consequence of this specific TRAF6 dimerization reveals unforeseen aspects of its E3 activity and mode of signal transduction.

## RESULTS

### Interaction with Ubc13 requires RING and zinc finger 1 (RZ<sub>1</sub>)

TRAF6-mediated Lys63-linked polyubiquitination requires the heterodimeric E2 complex of Ubc13 and Uev1A<sup>10</sup>. Whereas Ubc13 mediates

direct interaction with an E3, Uev1A provides the linkage specificity<sup>14,16-18</sup>. To understand how TRAF6 interacts with Ubc13, we constructed several deletion constructs of human TRAF6 containing the RING domain alone (residues 50-120), RZ<sub>1</sub> (residues 50-159, comprising RING and zinc finger 1), RZ<sub>12</sub> (residues 50-187, comprising RING and zinc fingers 1 and 2) and RZ<sub>123</sub> (residues 50-211, comprising RING and zinc fingers 1, 2 and 3). Unexpectedly, gel filtration chromatography analysis of complex formation showed that the RING domain alone was not sufficient for Ubc13 interaction (**Fig. 1b**). This is in contrast to many other RING domains that are necessary and sufficient for E2 interaction<sup>19</sup>. Instead, TRAF6 RZ<sub>1</sub> (residues 50-159) is the shortest construct that is necessary and sufficient for formation of a complex with Ubc13 (**Fig. 1b**). The first 49 residues of TRAF6 do not possess any recognizable domains and are dispensable for polyubiquitin synthesis (see below). They caused severe aggregation when included in any TRAF6 constructs.

We used surface plasmon resonance (SPR) to quantitatively measure the interaction between TRAF6 and Ubc13. An average  $K_d$  of approximately 1.6  $\mu$ M was obtained for the binding of Ubc13 to two coupling densities of TRAF6 RZ<sub>123</sub> (**Fig. 1c,d** and **Supplementary Fig. 1** online). This modest affinity is compatible with the necessity of an E2 to shuttle between its E1 and E3 (refs. 20,21). As seen in structure of the TRAF6-Ubc13 complex (below), substantial

**Table 1** Data collection, phasing and refinement statistics

	SeMet-TRAF6	TRAF6	TRAF6-Ubc13	TRAF6-Ubc13
<b>Data collection</b>				
Space group	<i>C</i> 2	<i>C</i> 2	<i>P</i> 1	<i>C</i> 2
Cell dimensions				
<i>a</i> , <i>b</i> , <i>c</i> (Å)	124.1, 81.1, 50.5	123.7, 80.8, 50.7	39.0, 42.8, 49.1	130.5, 41.4, 123.7
$\alpha$ , $\beta$ , $\gamma$ (°)	90.0, 91.5, 90.0	90.0, 91.4, 90.0	104.6, 99.6, 108.6	90.0, 116.2, 90.0
Resolution (Å)	50–2.6 (2.69–2.6)*	30–2.2 (2.28–2.2)*	50–2.1 (2.18–2.1)*	50–2.6 (2.69–2.6)*
<i>R</i> <sub>sym</sub>	0.074 (0.36)	0.074 (0.48)	0.050 (0.14)	0.046 (0.39)
<i>I</i> / $\sigma$ <i>I</i>	45.2 (6.9)	28.7 (2.9)	45.5 (9.3)	55.3 (5.1)
Completeness	0.97 (0.88)	0.98 (0.82)	0.96 (0.82)	0.99 (0.94)
Redundancy	5.7 (4.6)	6.4 (4.1)	3.9 (3.5)	6.8 (5.9)
<b>Refinement</b>				
Resolution (Å)		30–2.2	50–2.1	50–2.6
No. reflections		23,334	15,563	17,678
<i>R</i> <sub>work</sub> / <i>R</i> <sub>free</sub>		0.228 / 0.269	0.210 / 0.251	0.258 / 0.333
No. atoms				
Protein		2,520	2,018	4,062
Water		224	198	39
Average B-factors				
Protein (Å <sup>2</sup> )		51.2	47.1	80.6
Water (Å <sup>2</sup> )		68.7	57.3	63.4
r.m.s. deviations				
Bond lengths (Å)		0.006	0.006	0.008
Bond angles (°)		1.39	1.20	1.47

\*Values in parenthesis are for highest-resolution shell. One crystal was used for each data set.

contributions to the TRAF6–Ubc13 interaction are afforded by additional interactions from residues preceding the RING and by a structural role of the first zinc finger domain. The RING domain *per se* of TRAF6 shows weak affinity to Ubc13, as shown from NMR studies of the TRAF6 RING domain comprising residues 67–124 ( $K_d \approx 2$  mM)<sup>22</sup>.

### Elongated structure of TRAF6 RING and zinc fingers 1–3 (RZ<sub>123</sub>)

We determined the structure of human TRAF6 RZ<sub>123</sub> at 2.6-Å resolution by SAD and refined it to 2.2-Å resolution (Fig. 1e, Table 1 and Supplementary Fig. 2 online). The monomer structure is elongated and resembles the shape of a golf club, with the RING domain as the head (~35 Å in length) and the three zinc fingers as the shaft (~100 Å in length) (Fig. 1e). Unexpectedly, instead of beads on a string, the structure is rigid, as exemplified in the small r.m.s. deviation of 0.5 Å between the two independent, dimerically related TRAF6 molecules in the crystallographic asymmetric unit. The zinc fingers align in a linear fashion along the long axis of the molecule, with rotations of approximately 110° between the successive fingers (Fig. 1e). The fixed relationship between the successive fingers is at least partly due to the fixed sequence spacing between them. There are always three residues between the last cysteine residue of the previous finger to the first β-strand of the next finger (Fig. 1f and Supplementary Fig. 3 online). Together with the last cysteine in the previous finger, these three residues form a classical type I β-turn, which interacts with both zinc fingers to join them together. The region comprising the first and second zinc fingers of TRAF6 (Z<sub>12</sub>) is superimposable to the region comprising the second and third zinc fingers (Z<sub>23</sub>) with an r.m.s. deviation of 0.9 Å (Fig. 1g). The fourth zinc finger (Z<sub>4</sub>) can be modeled on the basis of its relationship with the previous zinc finger. This sequence spacing is conserved in different species of TRAF6 and in TRAF2, TRAF3 and TRAF5

(Supplementary Fig. 3), suggesting that it represents a conserved feature of the zinc finger arrangement in TRAFs.

### Structure of the TRAF6 RZ<sub>1</sub>–Ubc13 complex

We solved the structures of the human TRAF6 RZ<sub>1</sub>–Ubc13 complex independently in two crystal forms at 2.6-Å and 2.1-Å resolutions, respectively, by molecular replacement using the RZ<sub>1</sub> model from the TRAF6 RZ<sub>123</sub> structure and the previously determined Ubc13 structure<sup>16</sup> (Table 1 and Fig. 2a). As the structures are similar, with pairwise r.m.s. deviations of 0.8 Å, the description below is based on the higher-resolution structure. The TRAF6–Ubc13 complex buries approximately 1,000 Å<sup>2</sup> in surface area, most of which is hydrophobic (Figs. 1f and 2a,b). The architecture of the interaction is similar to the RING–E2 interaction in the c-Cbl–UbcH7 complex<sup>23</sup> and to the U-box–E2 interaction in the CHIP–Ubc13 complex<sup>24,25</sup>. RING and U-box domains share similar folds, but the latter do not coordinate any metal ions<sup>26</sup>.

Despite the general resemblance, a structural comparison showed that there is marked structural plasticity at these E3–E2 interfaces. This is true even when comparing the TRAF6–Ubc13 interaction with the CHIP–Ubc13 interaction, in

which Ubc13 is the E2 in both complexes. When TRAF6 is aligned with CHIP, Ubc13 molecules in the two complexes show rotational differences of approximately 10°. Some residues, such as Arg6 of Ubc13 at the interface with TRAF6, show C $\alpha$  position differences of up to 2 Å compared with the Ubc13 in complex with CHIP. Larger differences are also seen elsewhere in the Ubc13 structure. In addition, the interfacial residues show considerable side chain conformational variability (Supplementary Figs. 4 and 5 online).

In the TRAF6–Ubc13 complex, seven residues within the RING domain of TRAF6, Glu69, Pro71, Ile72, Leu74, Met75, Ala101 and Pro106, form the major contact site with Ubc13 (Figs. 1f and 2b). Among these interactions, Ile72 and Leu74 are completely buried at the interface and contribute the most surface area. Residues Ile72 and Leu74 of TRAF6 correspond to Ile236 and Phe238 of CHIP, respectively. Glu69 of TRAF6, which is Cys233 in CHIP, forms a salt bridge with Arg14 of Ubc13. In the CHIP–Ubc13 complex, the same Arg14 residue is hydrogen-bonded with Asp230 of CHIP (Supplementary Fig. 5).

Unexpectedly, in addition to the RING domain of TRAF6, residues preceding it (residues 54–66) contribute further to the Ubc13 interaction, which may be the reason for an enhanced affinity in comparison with the RING domain *per se*. At least two residues in this region, Gln54 and Asp57, form direct interactions with Ubc13, with Asp57 in salt bridges with Arg6 and Lys10 of Ubc13 (Fig. 2b). These interactions are completely absent in the CHIP–Ubc13 complex, and Arg6 of Ubc13 points to opposite directions in the two complexes. Involvement of Gln54 and Asp57 preceding the RING domain in the Ubc13 interaction revealed an indirect structural role of the first zinc finger in Ubc13 interaction. Residues 59–61 in the sequence preceding the RING domain form a β-strand (β<sub>1</sub>) that interacts with the β-hairpin (β<sub>5</sub> and β<sub>6</sub>) in the first zinc finger (Fig. 1e,f). This interaction is important for maintaining the proper conformation of the region for residues such as Gln54 and Asp57 to interact with

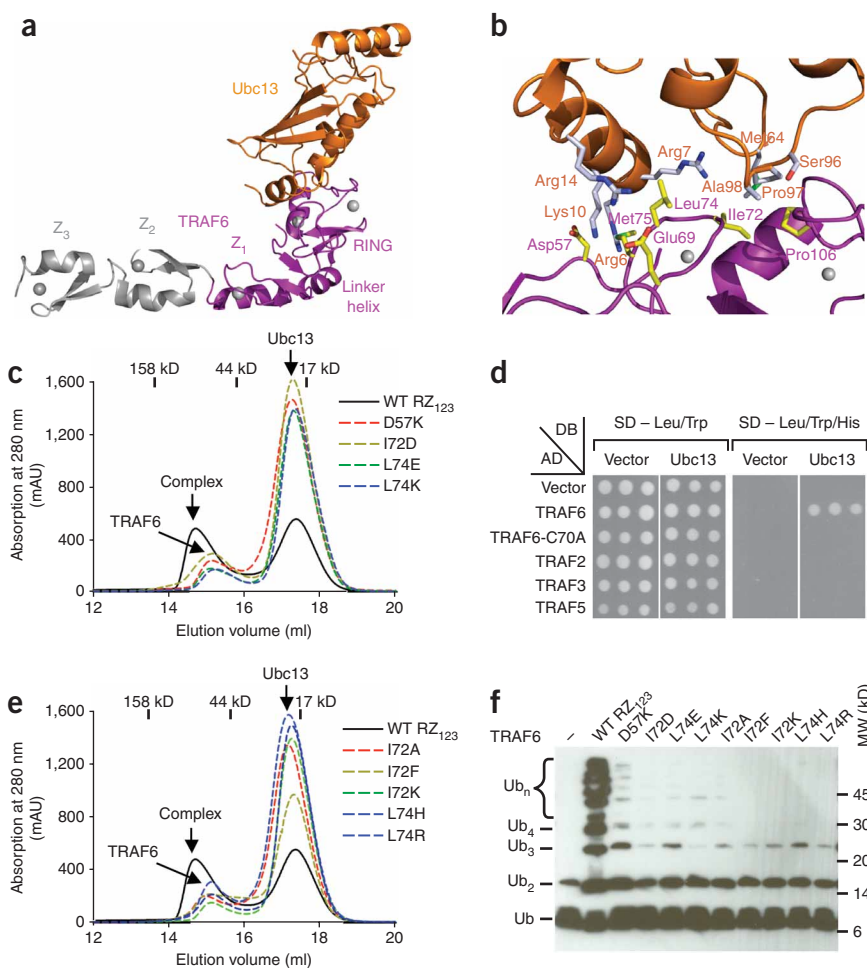


**Figure 2** Structural analysis of the TRAF6-Ubc13 interaction. **(a)** Ribbon diagram of the TRAF6 RZ<sub>1</sub>-Ubc13 complex. The Z<sub>2</sub> and Z<sub>3</sub> domains are modeled based on superposition of the TRAF6 RZ<sub>1</sub>-Ubc13 complex with the TRAF6 RZ<sub>123</sub> structure and are shown in gray. **(b)** Detailed interaction between TRAF6 and Ubc13. TRAF6 is shown in magenta with the carbon atoms of its side chains in yellow. Ubc13 is shown in orange with the carbon atoms of its side chains in gray. **(c)** Superimposed gel filtration profiles of Ubc13 mixed with wild-type (WT) or mutant TRAF6 RZ<sub>123</sub> designed to disrupt the interaction. Approximate elution positions of molecular weight standards are shown. **(d)** Yeast two-hybrid experiments on the interaction between Ubc13 and full-length TRAF2, TRAF3, TRAF5, TRAF6 (positive control) and its RING mutant C70A (negative control). **(e)** Superimposed gel filtration profiles of Ubc13 mixed with wild-type or mutant TRAF6 RZ<sub>123</sub> with interface residues switched to the corresponding sequences in other TRAFs: I72A (mutation to the corresponding TRAF2 sequence), I72K (TRAF3), I72F (TRAF5), L74H (TRAF3 and TRAF5) and L74R (TRAF2). Approximate elution positions of molecular weight standards are shown. **(f)** Promotion of polyubiquitin chain synthesis by wild-type and mutant TRAF6 RZ<sub>123</sub> in the presence of the E2 complex Ubc13-Uev1A and E1.

activation through Lys63-linked polyubiquitination<sup>2,27–29</sup>. Indeed, using yeast two-hybrid assays, we showed that full-length TRAF2, TRAF3 and TRAF5 did not interact with Ubc13, whereas TRAF6 interacted well with Ubc13 (**Fig. 2d**).

To understand the molecular basis for the lack of interactions, we generated mutations on TRAF6 that switch to the corresponding sequences in these TRAFs, I72A (TRAF2), I72K (TRAF3), I72F (TRAF5), L74H (TRAF3 and 5) and L74R (TRAF2) (**Fig. 1f**). Using gel filtration and yeast two-hybrid analyses, all these mutants were shown to be defective in their interactions with Ubc13 in comparison with the wild type (**Fig. 2e** and **Supplementary Fig. 6**), confirming that these substitutions could underlie the failure of these TRAFs to interact with Ubc13. Therefore, despite being in the same family of signaling proteins, TRAF2, TRAF3 and TRAF5 do not use the dimeric E2 Ubc13-Uev1A. Evolutionarily, TRAF6 is the oldest TRAF family member. It is likely that an initial ability to interact with Ubc13 became lost. One way that this loss may be compensated is through association with a Ubc13-interacting E3. In this regard, TRAF2 is known to be constitutively associated with the RING-containing proteins cIAP1 and cIAP2 (ref. 30). Sequence analysis predicts that cIAPs can interact with Ubc13 (**Supplementary Fig. 3**), and *in vitro* they promote polyubiquitination in the presence of Ubc13 (data not shown). These observations are consistent with recent reports describing the role of cIAPs in formation of the TNF receptor signaling complex<sup>31</sup> and the crucial roles of cIAPs in TNF-mediated NF- $\kappa$ B activation<sup>32</sup>.

**Polyubiquitin synthesis, autoubiquitination and NF- $\kappa$ B activation** Because many E3s promote polyubiquitin synthesis<sup>11</sup>, we tested the ability of TRAF6 to stimulate polyubiquitin chain assembly by the E2 complex Ubc13-Uev1A *in vitro*. TRAF6 RZ<sub>123</sub>, as well as RZ<sub>1</sub> and

Ubc13. The TRAF6 RING domain protein containing the preceding sequence but without the first zinc finger (RING, residues 50–120) did not form a complex with Ubc13 on gel filtration chromatography (**Fig. 1b**). Participation of residues preceding the RING in interaction with other E2s has also been observed in the c-Cbl complex with UbcH7 (ref. 23), in which the linker helix of c-Cbl contacts the similar N-terminal region of the E2.

### Mutagenesis confirms the TRAF6-Ubc13 interaction

We designed structure-based mutations on TRAF6 residues Ile72 and Leu74, which bury the most surface area at the interface, and on Asp57, a residue preceding the RING and contributing polar contacts with Ubc13. Mutations D57K, I72D, L74E and L74K were generated with the goal of disrupting the TRAF6-Ubc13 interaction. Gel filtration analysis using the TRAF6 RZ<sub>123</sub> protein showed that all mutants no longer interacted with Ubc13 (**Fig. 2c**). These results were further confirmed by yeast two-hybrid assays using full-length TRAF6 (**Supplementary Fig. 6** and **Supplementary Methods** online), demonstrating the importance of these residues in the Ubc13 interaction.

### Other TRAFs show undetectable interactions with Ubc13

Whereas all TRAF6 residues present at its interface with Ubc13 are conserved among sequences from different species, most are not conserved in TRAF2, TRAF3 and TRAF5 (**Fig. 1f**). This is unexpected because at least TRAF2 and TRAF5 are known to mediate NF- $\kappa$ B

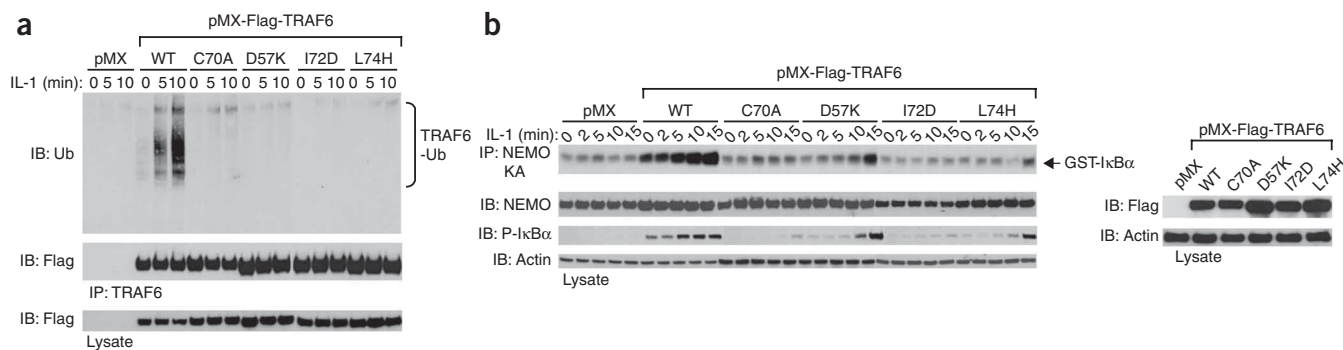


**Figure 3** Cellular effects of TRAF6 mutants that fail to interact with Ubc13. (a) TRAF6 mutants defective in Ubc13 interaction failed to rescue IL-1–induced TRAF6 autoubiquitination in TRAF6-deficient MEFs. The indicated stable cells lines were treated with IL-1 (1 ng ml<sup>-1</sup>) for the indicated times and the clarified lysates were immunoblotted with the indicated antibodies. (b) TRAF6 mutants defective in Ubc13 interaction failed to rescue IL-1–induced IKK activation and IκB phosphorylation in *Traf6*<sup>-/-</sup> MEFs. IB, immunoblot; WT, wild type.

RZ<sub>123</sub> (residues 50–279), strongly promoted polyubiquitin chain synthesis in the presence of E1, E2, ubiquitin and ATP (Fig. 2f and data not shown). The interaction between TRAF6 and Ubc13 is required, as TRAF6 mutants generated to disrupt the interaction or to mimic other TRAFs were all defective in promoting polyubiquitin chain synthesis (Fig. 2f).

TRAF6 undergoes autoubiquitination upon receptor stimulation by ligands such as IL-1, and this autoubiquitination is required for NF-κB activation<sup>8</sup>. To determine whether the observed TRAF6–Ubc13 interaction is also required for TRAF6 autoubiquitination and NF-κB activation upon stimulation, we used wild-type and mutant TRAF6 to rescue *Traf6*-deficient mouse embryonic fibroblasts (MEFs). Retroviral infection of wild-type TRAF6 rescued TRAF6 autoubiquitination upon IL-1 treatment (Fig. 3a). In contrast to the wild type, TRAF6 with mutations disrupting the Ubc13 interaction failed to rescue TRAF6 autoubiquitination in response to IL-1 (Fig. 3a). Furthermore, we determined whether IKK was activated in these cells by pulling down IKK using antibody against the IKK-regulatory subunit NEMO. *In vitro* kinase assay in phosphorylating purified GST-IκBα showed that IKK was active only in MEFs infected with wild-type TRAF6, and not with Ubc13 binding-defective TRAF6 mutants (Fig. 3b). These data support a crucial role of the observed Ubc13 interaction in TRAF6 function in cells.

### TRAF6 dimerization in the crystal and in solution

The N-terminal region of TRAF6 forms a markedly elongated non-crystallographic dimer in the crystal (Fig. 4a). We did not anticipate this, because the C-terminal coiled coil and TRAF-C domains form trimeric structures<sup>3,4,6,7</sup>. The dimeric N-terminal domain of TRAF6 causes a symmetry mismatch in the full-length TRAF6 structure. The dimerization interface is formed via the RING and part of the linker helix α2, and buries a total of 1,270 Å<sup>2</sup> in surface area, most of which is hydrophobic (Figs. 1f and 4a,b). Along the two-fold axis, the solvent-exposed hydrophobic side chains of Phe118 of both monomers stack against each other and probably form the core of the interface. At the adjacent region, Lys67, Gln82, Arg88 and Phe122 form another patch of the interface.

We generated potentially disruptive TRAF6 mutations F118A, F122A, R88A and the double mutation R88A F122A, as well as the more conservative substitutions F118Y and F118W on TRAF6 RZ<sub>123</sub>. In comparison with wild-type RZ<sub>123</sub>, the gel filtration elution positions of F118A, R88A and the R88A F122A mutants of TRAF6 RZ<sub>123</sub> shifted toward a lower molecular weight (Fig. 4c). This suggests that

the F118A, R88A and the R88A F122A mutations disrupted TRAF6 dimerization. The elution position of F118Y shifted slightly toward a lower molecular weight, suggesting that it is partially defective in dimerization.

To determine whether the TRAF6 dimer in solution is the elongated dimer we observed in the crystal (Fig. 4a), we performed small-angle X-ray scattering (SAXS) on the wild-type RZ<sub>123</sub> protein of TRAF6 and its F118A mutant. The scattering profile from wild-type TRAF6 was used to derive its global shape parameters, such as the overall radius of gyration, the maximum dimension and the radius of gyration of the cross-section. These model-independent, experimentally derived parameters showed excellent agreement with those calculated from the dimeric, but not the monomeric, TRAF6 crystal structure (Fig. 4d). Low-resolution shape reconstruction from the SAXS data of the wild-type TRAF6 showed an elongated molecular envelope that superimposes well with the dimeric TRAF6 structure (Fig. 4e). The only region of TRAF6 that protrudes outside the molecular envelope corresponds to the α1-β4 loop, a region with high B-factors in the crystal.

We analyzed the scattering profiles measured from wild-type and the F118A mutant TRAF6 by comparing them against those calculated from the crystal structures (Fig. 4f). The  $\chi^2$  value, as defined in the program CRYSOLOG<sup>33</sup>, was used as a metric of agreement. For wild-type TRAF6, the scattering profile matched that calculated from the dimeric crystal structure, with a good  $\chi^2$  agreement of 1.41, whereas that from a monomer gave a poor  $\chi^2$  agreement of 11.2. The SAXS curve of the F118A mutant fit to a mixture of 44% monomer and 56% dimer, with a good  $\chi^2$  agreement of 1.30. As compared with that from the gel filtration profile, this apparent higher dimeric proportion may be due to the much higher protein concentration used in the SAXS measurement. These data demonstrated that TRAF6 exists as the elongated dimer in solution.

### TRAF6 dimerization is crucial for its biological functions

Given the dimeric structure of TRAF6, we wondered whether this dimerization is important for TRAF6 function. Notably, residues at the dimerization interface are much more conserved than residues for Ubc13 interaction (Fig. 1f). They are conserved not only among the different species of TRAF6 but also among TRAF2, TRAF3 and TRAF5. Unexpectedly, TRAF6 RZ<sub>123</sub> mutants with defective dimerization were impaired in their ability to promote polyubiquitin chain synthesis *in vitro* (Fig. 4g). The three TRAF6 mutants that

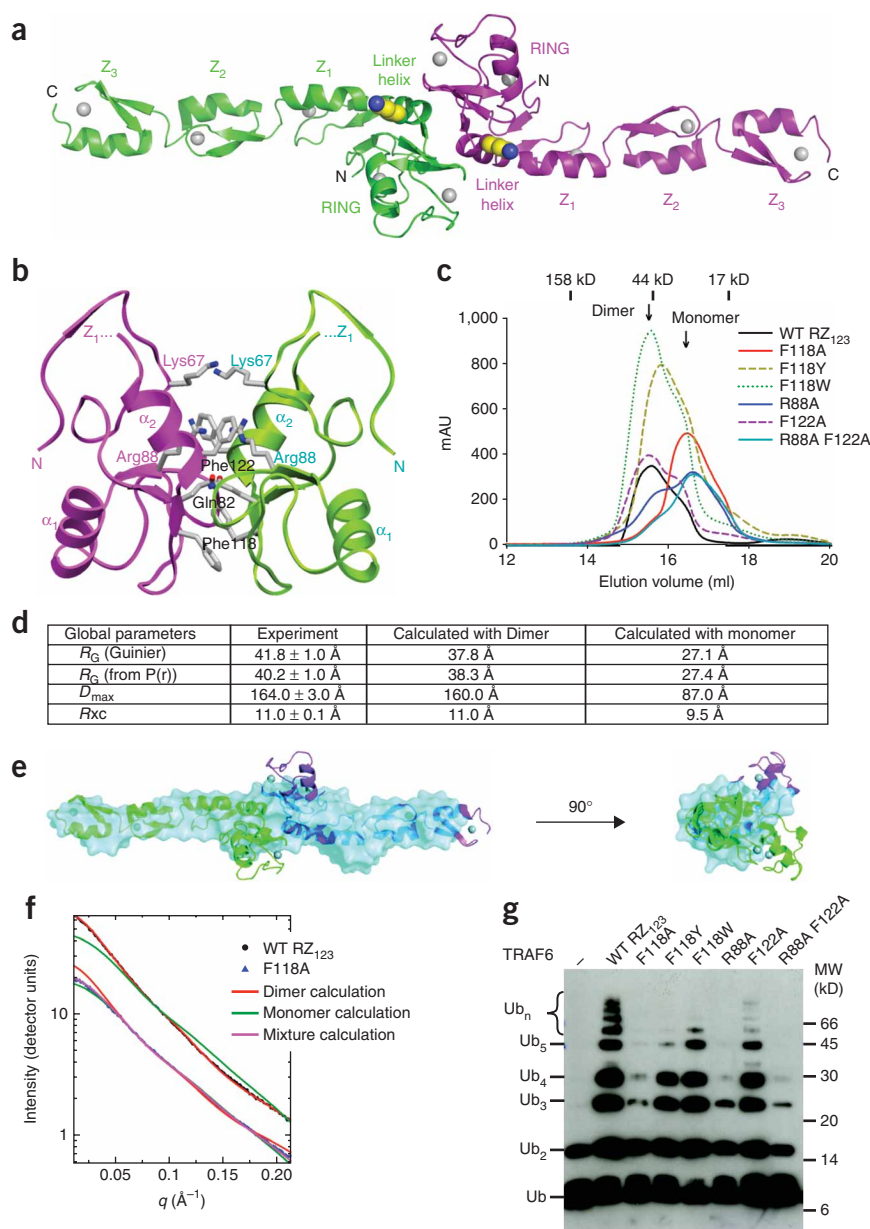


**Figure 4** TRAF6 dimerization is crucial for its ability to promote polyubiquitin chain synthesis. **(a)** Dimeric structure of TRAF6 RZ<sub>123</sub>, shown with the two-fold axis perpendicular to the page. The major autoubiquitination residue, Lys124, is shown in ball-and-stick model. **(b)** Detailed interactions at the TRAF6 dimerization interface. **(c)** Superimposed gel filtration profiles of wild-type (WT) and dimerization mutants of TRAF6 RZ<sub>123</sub>. **(d)** Global shape parameters ( $\pm$  s.e.m) derived from SAXS of wild-type TRAF6 RZ<sub>123</sub> and in comparison with those calculated from monomeric and dimeric TRAF6 crystal structure. **(e)** Solution structure from SAXS data on TRAF6 Z<sub>123</sub>. The averaged SAXS envelope (cyan) generated from ten independent runs of DAMMIN<sup>44</sup> is overlaid on the crystallographic dimer shown in a ribbon representation. DAMMIN fits the scattering data directly and does not require the number of amino acids as an input. In addition, no assumptions on symmetry were applied. **(f)** Experimental and calculated scattering profiles from the wild-type and the F118A mutant of TRAF6 RZ<sub>123</sub>. The experimental scattering profile from the wild-type TRAF6 (black circles) is well fit by the scattering profile calculated from the dimer found in the crystal structure (red) and poorly fit by the monomer (green). The experimental scattering profile from the F118A mutant (blue triangles, and artificially scaled down for clarity) is best fit by a mixture of monomers and dimers (magenta).  $q = 4\pi \sin(\theta/2)/\lambda$ , where  $\theta$  is the scattering angle and  $\lambda$  is the wavelength. **(g)** Promotion of polyubiquitin chain synthesis by wild-type and dimerization mutants of TRAF6 RZ<sub>123</sub>. Ub, ubiquitin.

protrudes away from the interface (Fig. 4a). In fact, the K124R mutant with defective TRAF6 autoubiquitination<sup>8</sup> is still dimeric and interacts with Ubc13 (data not shown). Consistent with the defective autoubiquitination, dimerization mutants of TRAF6 also showed impaired abilities to restore IKK activation in *Traf6*<sup>-/-</sup> MEFs (Fig. 5b). The R88A F122A mutant was the most defective, with R88A and F118A showing residual and delayed IKK activation, consistent with the severity of impairment in polyubiquitin synthesis *in vitro* (Fig. 4g).

#### TRAF6 dimerization induces higher-order oligomerization

Because the C-terminal region of TRAF6 is trimeric, we wondered what kind of oligomer is formed by full-length TRAF6 and what would be the consequences of disrupting dimerization. To answer these questions, we fused TRAF6 to the N terminus of Cerulean or Venus and performed fluorescence resonance energy transfer (FRET) experiments. When BJAB lymphoma cells were co-transfected with wild-type TRAF6-Cerulean and TRAF6-Venus fusion constructs, we observed intense FRET signals (Fig. 6a). In contrast, co-transfection of the F118A-Venus fusion construct with either wild-type TRAF6-Cerulean or F118A-Cerulean, yielded much lower FRET signals (Fig. 6a). The larger FRET signals correlated with a spontaneous aggregation seen under confocal microscopy of wild-type TRAF6 in BJAB cells upon expression of the fusion constructs (data not shown).

were most defective in dimerization, F118A, R88A and R88A F122A, were severely impaired in polyubiquitin synthesis, with R88A F122A being the most impaired. F118Y was partially impaired in its ability to promote polyubiquitin formation, consistent with its partial defectiveness in dimerization. Therefore, there was a high correlation between the dimerization tendencies of wild-type and mutant TRAF6 and their E3 activities. The TRAF6 dimerization interface lies away from the Ubc13 interaction interface, and we confirmed the ability of the dimerization mutants to interact with Ubc13 (Supplementary Fig. 7 online).

TRAF6 is both an E3 and a substrate that undergoes functionally important autoubiquitination<sup>8</sup>. Full-length TRAF6 defective in dimerization also failed to undergo autoubiquitination (Fig. 5a). The major autoubiquitination site in TRAF6 has been mapped to Lys124 (ref. 8), which resides on the linker helix between the RING domain and the first zinc finger domain (Fig. 1f). Although Lys124 resides on the same linker helix involved in dimerization, its side chain

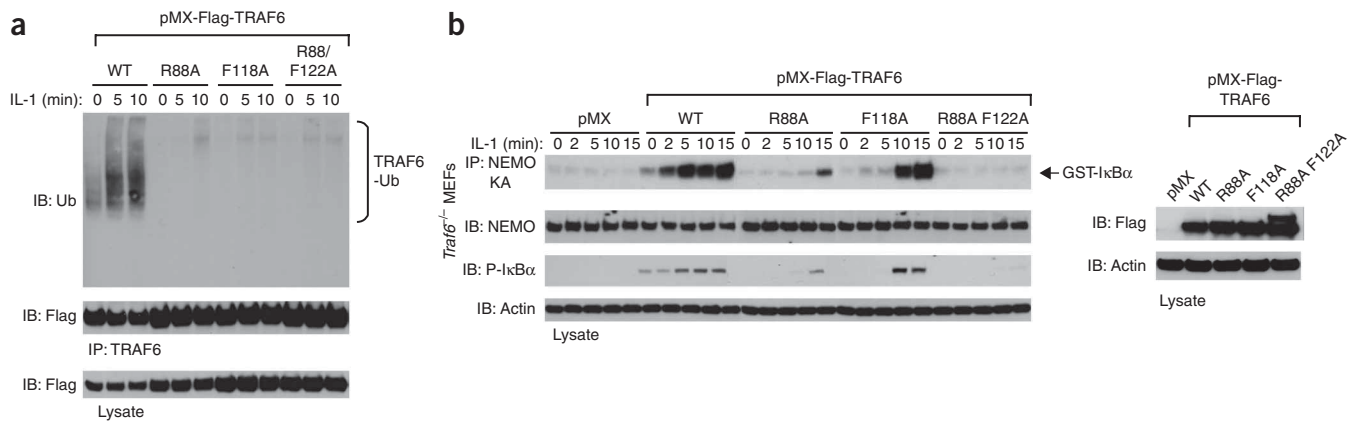


**Figure 5** Cellular effects of TRAF6 mutants that fail to dimerize. **(a)** TRAF6 dimerization mutants failed to rescue IL-1-induced TRAF6 autoubiquitination in TRAF6-deficient MEFs. The indicated stable cell lines were treated with IL-1 ( $1 \text{ ng ml}^{-1}$ ) for the indicated times and the clarified lysates were immunoblotted with the indicated antibodies. **(b)** TRAF6 dimerization mutants failed to rescue IL-1-induced IKK activation and  $\text{I}\kappa\text{B}$  phosphorylation. IB, immunoblot; Ub, ubiquitin; WT, wild type.

In contrast, the F118A mutant fusion constructs gave only a smeared expression pattern, suggesting that TRAF6 dimerization is also crucial for higher-order oligomerization of TRAF6.

To determine whether spontaneous aggregation upon receptor stimulation also occurs under endogenous conditions, we used lipopolysaccharides (LPS) to stimulate Toll-like receptors on B220

cells. We detected endogenous TRAF6 using anti-TRAF6 antibody followed by visualization with an AlexaFluor568-coupled secondary antibody. Comparison of TRAF6 distribution before and after LPS treatment showed a clear coalescence of TRAF6 in discernable clusters to the cell surface upon activation (**Fig. 6b,c**). The fact that the coalescence is visible microscopically suggests that many

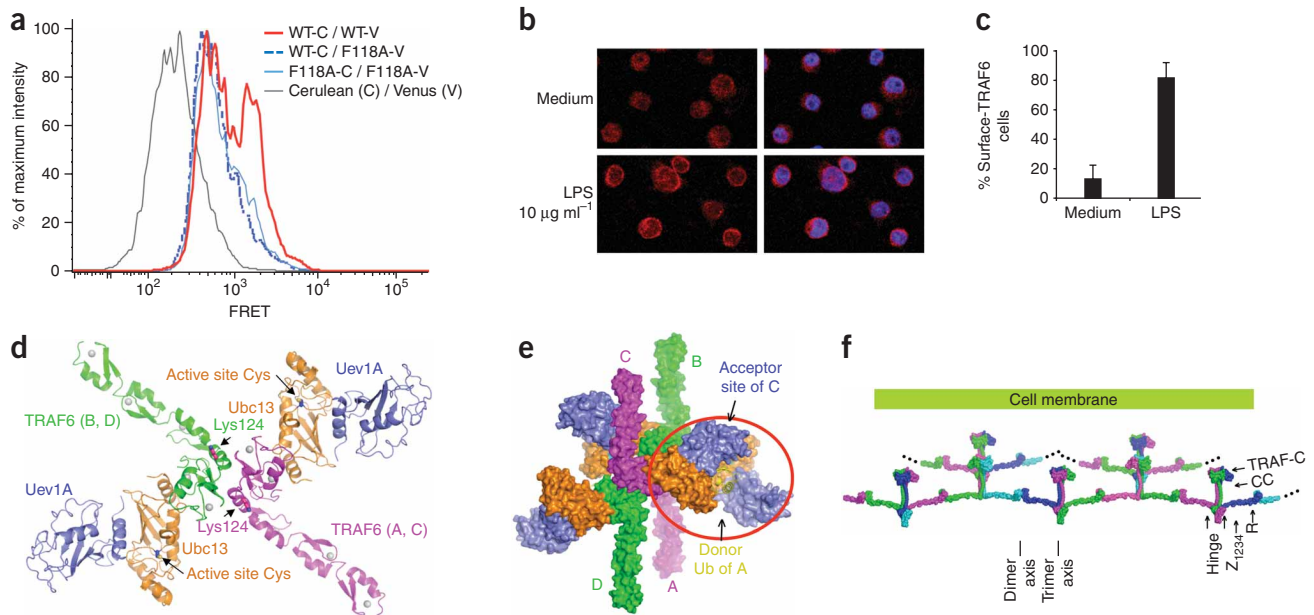


**Figure 6** TRAF6 oligomerization. **(a)** Measurement of TRAF6 self-association by FRET. B220 lymphoma cells were co-transfected with Cerulean (C) and Venus (V) fusion constructs for expressing wild-type (WT) or F118A mutant TRAF6 fusion proteins as indicated. The intensity of FRET signals were determined by flow cytometry, gating on live Cerulean positive cells that had been excited by a 407-nm laser and measuring emission post a 550/50 nm band-pass filter. **(b)** Endogenous TRAF6 aggregation at the cell surface during signaling. Distribution of intracellular TRAF6 (red) in B220 cells changes from diffused toward membranous condensed patterns upon LPS stimulation for 2 h. Hoechst 33342 (blue) specifies nuclei. **(c)** The percentages of cells having surface TRAF6 in unstimulated and LPS-stimulated samples are shown. Data represent more than 10 images from 3 independent experiments. Error bars represent s.d. **(d)** A dimeric TRAF6-Ubc13-Uev1A complex built based on the dimeric TRAF6 structure, the dimeric TRAF6-Ubc13 structure and the Ubc13-Mms2 structure<sup>14</sup>. TRAF6 autoubiquitination sites at Lys124 and the active site locations of Ubc13 are shown. **(e)** A potential tetrameric assembly of the TRAF6-Ubc13-Uev1A complex mediated by the interaction between a loaded ubiquitin (Ub) on Ubc13 (yellow, stick model) of one dimeric complex and an acceptor site on Uev1A of another dimeric complex. **(f)** A model of oligomerized full-length TRAF6 in the activated state, showing the potential for infinite aggregation. TRAF6 is shown in four alternative colors (magenta, green, cyan and blue) and is modeled by piecing together the N-terminal region structure and the C-terminal region structure. Zinc finger 4 is modeled based on its predicted relationship with zinc finger 3. The linker between zinc finger 4 and the coiled coil may act as a flexible hinge.

individual TRAF6 molecules participate in this signaling-induced aggregation, similar to the spontaneous aggregation observed under TRAF6 overexpression.

## DISCUSSION

RING domains and their variants may constitute the largest family of ubiquitin ligases<sup>19</sup>. The established concept is that the RING interacts with E2 to bring the substrate to the proximity of E2 for ubiquitination. Our studies show that the RING of TRAF6 does not function alone, but instead functions together with the neighboring sequences in TRAF6, including the residues preceding the RING and involving a structural role of the first zinc finger. Despite the availability of several E2–E3 complex structures<sup>26,27</sup>, these details in the interaction of TRAF6 with Ubc13 could not have been predicted. Unexpectedly, this interaction is specific for TRAF6, but not other members of the TRAF family, perhaps highlighting the unique critical biological roles of TRAF6 in multiple receptor signaling pathways.

Despite the trimeric symmetry of the C-terminal domain of TRAF6, the N-terminal domain of TRAF6 is dimerized via its RING domain and the linker helix to enable the formation of a dimeric TRAF6–Ubc13–Uev1A complex (Fig. 6d). Although RING dimerization has been observed before<sup>34,35</sup>, its functional consequence has not been fully investigated. In the case of TRAF6, dimerization is important for its ability to promote polyubiquitin synthesis, autoubiquitination and NF- $\kappa$ B activation and correlates with its higher-order oligomerization. However, how TRAF6 dimerization facilitates these activities remains to be elucidated. For synthesizing long polyubiquitin chains, it is crucial to preferentially re-use polyubiquitin intermediates in the following cycle of ubiquitination. Therefore, a simplest explanation might be that TRAF6 dimerization results in an increased local concentration of the Ubc13–Uev1A complex to trap locally generated polyubiquitin intermediates. Heterologous dimerization has been shown to activate the E2 cdc34 E2 directly in the absence of E3 (ref. 36). In addition, when Ubc13 is loaded with donor ubiquitin, the E2–E3 complex dimers may further tetramerize through the low-affinity interaction between Uev1A and the ubiquitin<sup>14</sup> (Fig. 6e). Ubiquitin-loaded E2 UbcH5 has been shown to have a tendency to form oligomers, which is required for processive BRCA1-directed ubiquitination<sup>37</sup>.

In the case of TRAF6 autoubiquitination, it is possible that dimerization of the TRAF6 N-terminal region is required because it promotes higher-order aggregation. We have shown that the N-terminal region *per se* is not sufficient for TRAF6 autoubiquitination in cells; instead, the trimeric coiled coil region is also needed (data not shown). On the molecular level, the observed higher-order aggregation of TRAF6 is consistent with an infinite expandable model of full-length TRAF6 in its activated state as a consequence of the symmetry mismatch between its N- and C-terminal regions. In this model, the dimeric and trimeric symmetry axes are roughly parallel to each other, and both are perpendicular to the membrane surface to enable multiple engagements of receptor trimers (Fig. 6f). The size of the aggregate may depend on TRAF6 concentration, receptor engagement and interaction with other signaling proteins in the cell. Both dimerization and trimerization would cooperate in this model to form the lattice of interactions, and the expanded lattice would in turn strengthen dimerization and trimerization. It is likely that the lattice of interactions, and the inherent flexibility at the N- and C-terminal region junctions, provides the necessary geometry required for transfer of polyubiquitin chains, *in trans*, from one E2 to the TRAF6 autoubiquitination site at Lys124 of another TRAF6–E2 complex.

In the context of this model, the difference in FRET signals between wild-type TRAF6 and the F118A mutant may have resulted from stabilization of TRAF6 trimerization in the expanded lattice of interactions. The distance between the C terminus of TRAF6 in the protomers of the trimer is approximately 26 Å in the crystal structure of the C-terminal region of TRAF6 (refs. 3,5), whereas the estimated distance between dimerically related C termini is more than 200 Å. Alternatively, because the linker region between the end of zinc finger 4 and the beginning of the coiled coil is predicted to lack secondary structures and may, therefore, be flexible, it is also possible that different C-terminal trimers are also brought into close proximity as well in this higher-order aggregation, leading to enhanced FRET signals.

Therefore, our studies have not only unveiled interesting aspects of TRAF6 E2 interaction and dimerization, but also revealed an unexpected platform of oligomerization in mediating TRAF6 function. The massive increase in local concentrations of the associated signaling proteins in this aggregation platform probably acts as a factory to promote polyubiquitin synthesis, autoubiquitination and recruitment of downstream proteins such as the TAK1 complex and the IKK complex. In keeping with this concept, recent studies suggest that the crucial role of oligomerization in ubiquitination in general may be more prevalent than previously anticipated<sup>38–40</sup>. Notably, the proposed model of TRAF6 aggregation bears unexpected similarity to assembly of the death receptor signaling complex upon activation of Fas, a death receptor in the TNF receptor superfamily<sup>41–43</sup>. The aggregations in both systems could provide an elegant scaffold to facilitate proximity-induced caspase activation, ubiquitination or kinase activation. On a conceptual level, these observations signify a convergence of the signaling mechanisms of caspase-mediated death pathways and the TRAF-mediated survival pathways in immune receptor signal transduction.

## METHODS

Methods and any associated references are available in the online version of the paper at <http://www.nature.com/nsmb/>.

**Accession codes.** Protein Data Bank: Coordinates for TRAF6 and the TRAF6/Ubc13 complex in two crystal forms have been deposited with accession codes 3HCS, 3HCT and 3HCU, respectively.

*Note: Supplementary information is available on the Nature Structural & Molecular Biology website.*

## ACKNOWLEDGMENTS

We thank T. Min and J.Y. Chung for their earlier work on the project, X. Jiang and X. Wang of the Sloan-Kettering Institute for purified E1, Z. Chen of the University of Texas Southwestern Medical School for the expression constructs of Ubc13 and Uev1A, R. Abramowitz and J. Schwanof of X4A of the National Synchrotron Light Source for data collection and J. Wu for maintaining our X-ray and computer equipment. This work was supported by the US National Institutes of Health (RO1 AI045937 to H.W. and RO1 AR053540 to B.G.D.), the US Department of Defense (DOE Contract DE-AC02-05CH11231 for G.H.), the Intramural Research Program of the US National Institute of Allergy and Infectious Diseases (to L.Z. and M.J.L.) and institutional start-up funds to B.G.D., S.-C.L. and Y.-C.L. from the Cancer Research Institute and to M.L. from the American Heart Association.

Published online at <http://www.nature.com/nsmb/>

Reprints and permissions information is available online at <http://npg.nature.com/reprintsandpermissions/>

1. Wu, H. Assembly of post-receptor signaling complexes for the tumor necrosis factor receptor superfamily. *Adv. Protein Chem.* **68**, 225–279 (2004).
2. Pineda, G., Ea, C.K. & Chen, Z.J. Ubiquitination and TRAF signaling. *Adv. Exp. Med. Biol.* **597**, 80–92 (2007).

3. Park, Y.C., Burkitt, V., Villa, A.R., Tong, L. & Wu, H. Structural basis for self-association and receptor recognition of human TRAF2. *Nature* **398**, 533–538 (1999).
4. McWhirter, S.M. *et al.* Crystallographic analysis of CD40 recognition and signaling by human TRAF2. *Proc. Natl. Acad. Sci. USA* **96**, 8408–8413 (1999).
5. Ye, H. *et al.* Distinct molecular mechanism for initiating TRAF6 signalling. *Nature* **418**, 443–447 (2002).
6. Deng, L. *et al.* Activation of the I $\kappa$ B kinase complex by TRAF6 requires a dimeric ubiquitin-conjugating enzyme complex and a unique polyubiquitin chain. *Cell* **103**, 351–361 (2000).
7. Wang, C. *et al.* TAK1 is a ubiquitin-dependent kinase of MKK and IKK. *Nature* **412**, 346–351 (2001).
8. Lamothe, B. *et al.* Site-specific Lys-63-linked tumor necrosis factor receptor-associated factor 6 auto-ubiquitination is a critical determinant of I $\kappa$ B kinase activation. *J. Biol. Chem.* **282**, 4102–4112 (2007).
9. Hershko, A. & Ciechanover, A. The ubiquitin system. *Annu. Rev. Biochem.* **67**, 425–479 (1998).
10. Pickart, C.M. & Eddins, M.J. Ubiquitin: structures, functions, mechanisms. *Biochim. Biophys. Acta* **1695**, 55–72 (2004).
11. Hochstrasser, M. Lingering mysteries of ubiquitin-chain assembly. *Cell* **124**, 27–34 (2006).
12. Dye, B.T. & Schulman, B.A. Structural mechanisms underlying posttranslational modification by ubiquitin-like proteins. *Annu. Rev. Biophys. Biomol. Struct.* **36**, 131–150 (2007).
13. Pickart, C.M. & Fushman, D. Polyubiquitin chains: polymeric protein signals. *Curr. Opin. Chem. Biol.* **8**, 610–616 (2004).
14. Eddins, M.J., Carlile, C.M., Gomez, K.M., Pickart, C.M. & Wolberger, C. Mms2-Ubc13 covalently bound to ubiquitin reveals the structural basis of linkage-specific polyubiquitin chain formation. *Nat. Struct. Mol. Biol.* **13**, 915–920 (2006).
15. Chen, Z.J. Ubiquitin signalling in the NF- $\kappa$ B pathway. *Nat. Cell Biol.* **7**, 758–765 (2005).
16. VanDemark, A.P., Hofmann, R.M., Tsui, C., Pickart, C.M. & Wolberger, C. Molecular insights into polyubiquitin chain assembly: crystal structure of the Mms2/Ubc13 heterodimer. *Cell* **105**, 711–720 (2001).
17. Moraes, T.F. *et al.* Crystal structure of the human ubiquitin conjugating enzyme complex, hMms2-hUbc13. *Nat. Struct. Biol.* **8**, 669–673 (2001).
18. McKenna, S. *et al.* Noncovalent interaction between ubiquitin and the human DNA repair protein Mms2 is required for Ubc13-mediated polyubiquitination. *J. Biol. Chem.* **276**, 40120–40126 (2001).
19. Ardley, H.C. & Robinson, P.A. E3 ubiquitin ligases. *Essays Biochem.* **41**, 15–30 (2005).
20. Eletr, Z.M., Huang, D.T., Duda, D.M., Schulman, B.A. & Kuhlman, B. E2 conjugating enzymes must disengage from their E1 enzymes before E3-dependent ubiquitin and ubiquitin-like transfer. *Nat. Struct. Mol. Biol.* **12**, 933–934 (2005).
21. Huang, D.T. *et al.* Structural basis for recruitment of Ubc12 by an E2 binding domain in NEDD8's E1. *Mol. Cell* **17**, 341–350 (2005).
22. Mercier, P. *et al.* Structure, interactions, and dynamics of the RING domain from human TRAF6. *Protein Sci.* **16**, 602–614 (2007).
23. Zheng, N., Wang, P., Jeffrey, P.D. & Pavletich, N.P. Structure of a c-Cbl-UbcH7 complex: RING domain function in ubiquitin-protein ligases. *Cell* **102**, 533–539 (2000).
24. Zhang, M. *et al.* Chaperoned ubiquitylation—crystal structures of the CHIP U box E3 ubiquitin ligase and a CHIP-Ubc13-Uev1a complex. *Mol. Cell* **20**, 525–538 (2005).
25. Xu, Z. *et al.* Structure and interactions of the helical and U-box domains of CHIP, the C terminus of HSP70 interacting protein. *Biochemistry* **45**, 4749–4759 (2006).
26. Ohi, M.D., Vander Kooi, C.W., Rosenberg, J.A., Chazin, W.J. & Gould, K.L. Structural insights into the U-box, a domain associated with multi-ubiquitination. *Nat. Struct. Biol.* **10**, 250–255 (2003).
27. Rothe, M., Wong, S.C., Henzel, W.J. & Goeddel, D.V. A novel family of putative signal transducers associated with the cytoplasmic domain of the 75 kDa tumor necrosis factor receptor. *Cell* **78**, 681–692 (1994).
28. Nakano, H. *et al.* TRAF5, an activator of NF- $\kappa$ B and putative signal transducer for the lymphotoxin- $\beta$  receptor. *J. Biol. Chem.* **271**, 14661–14664 (1996).
29. Ishida, T.K. *et al.* TRAF5, a novel tumor necrosis factor receptor-associated factor family protein, mediates CD40 signalling. *Proc. Natl. Acad. Sci. USA* **93**, 9437–9442 (1996).
30. Rothe, M., Pan, M.G., Henzel, W.J., Ayres, T.M. & Goeddel, D.V. The TNFR2-TRAF signalling complex contains two novel proteins related to baculoviral inhibitor of apoptosis proteins. *Cell* **83**, 1243–1252 (1995).
31. Santoro, M.M., Samuel, T., Mitchell, T., Reed, J.C. & Stainier, D.Y. Birc2 (clap1) regulates endothelial cell integrity and blood vessel homeostasis. *Nat. Genet.* **39**, 1397–1402 (2007).
32. Mahoney, D.J. *et al.* Both cIAP1 and cIAP2 regulate TNF $\alpha$ -mediated NF- $\kappa$ B activation. *Proc. Natl. Acad. Sci. USA* **105**, 11778–11783 (2008).
33. Svergun, D., Barabero, C. & Koch, M.H. CRYSOLE—a program to evaluate X-ray solution scattering of biological macromolecules from atomic coordinates. *J. Appl. Cryst.* **28**, 768–773 (1995).
34. Kostic, M., Matt, T., Martinez-Yamout, M.A., Dyson, H.J. & Wright, P.E. Solution structure of the Hdm2 C2H2C4 RING, a domain critical for ubiquitination of p53. *J. Mol. Biol.* **363**, 433–450 (2006).
35. Knipscheer, P. & Sixma, T.K. Protein-protein interactions regulate Ubl conjugation. *Curr. Opin. Struct. Biol.* **17**, 665–673 (2007).
36. Gazdoui, S. *et al.* Proximity-induced activation of human Cdc34 through heterologous dimerization. *Proc. Natl. Acad. Sci. USA* **102**, 15053–15058 (2005).
37. Brzovic, P.S., Lissounov, A., Christensen, D.E., Hoyt, D.W. & Klevit, R.E.A. UbcH5/ubiquitin noncovalent complex is required for processive BRCA1-directed ubiquitination. *Mol. Cell* **21**, 873–880 (2006).
38. Hao, B., Oehlmann, S., Sowa, M.E., Harper, J.W. & Pavletich, N.P. Structure of a Fbw7-Skp1-cyclin E complex: multisite-phosphorylated substrate recognition by SCF ubiquitin ligases. *Mol. Cell* **26**, 131–143 (2007).
39. Tang, X. *et al.* Suprafacial orientation of the SCFCdc4 dimer accommodates multiple geometries for substrate ubiquitination. *Cell* **129**, 1165–1176 (2007).
40. Peschard, P. *et al.* Structural basis for ubiquitin-mediated dimerization and activation of the ubiquitin protein ligase Cbl-b. *Mol. Cell* **27**, 474–485 (2007).
41. Yang, J.K. *et al.* Crystal structure of MC159 reveals molecular mechanism of DISC assembly and FLIP inhibition. *Mol. Cell* **20**, 939–949 (2005).
42. Carrington, P.E. *et al.* The structure of FADD and its mode of interaction with procaspase-8. *Mol. Cell* **22**, 599–610 (2006).
43. Siegel, R.M. *et al.* SPOTS: signaling protein oligomeric transduction structures are early mediators of death receptor-induced apoptosis at the plasma membrane. *J. Cell Biol.* **167**, 735–744 (2004).
44. Svergun, D.I. Restoring low resolution structure of biological macromolecules from solution scattering using simulated annealing. *Biophys. J.* **76**, 2879–2886 (1999).

## ONLINE METHODS

**Protein expression, purification and mutagenesis.** We constructed human TRAF6 RING (residues 50–120), RZ<sub>1</sub> (residues 50–159), RZ<sub>12</sub> (residues 50–187), RZ<sub>123</sub> (residues 50–211) and RZ<sub>1234</sub> (residues 50–279) with C-terminal polyhistidine (His<sub>6</sub>) tags and human Ubc13 and Uev1A with N-terminal His<sub>6</sub> tags. We expressed these proteins in BL21-CodonPlus (DE3) cells and purified them by Ni<sup>2+</sup>-affinity chromatography (Qiagen) and gel filtration chromatography (Superdex 200, GE Healthcare). We removed the N-terminal His<sub>6</sub> tags by thrombin (GE Healthcare) cleavage. To obtain the Ubc13–Uev1A complex, we mixed equimolar purified tagless Ubc13 and Uev1A and passed the mixture through the gel filtration column. For complex formation with Ubc13, we incubated a given TRAF6 construct (concentrations from 0.16 mM to 0.6 mM) with excess Ubc13 (molar ratios from 1:1.2 to 1:2) for gel filtration chromatography. Injection volumes ranged from 450  $\mu$ l to 735  $\mu$ l. We performed mutagenesis using the QuikChange Site-Directed Mutagenesis Kit (Stratagene).

**Crystallization and structure determination.** We crystallized TRAF6 RZ<sub>123</sub> and the RZ<sub>1</sub>–Ubc13 complex using hanging drop vapor diffusion at 20 °C. The crystallization conditions for RZ<sub>123</sub> were 1.19–1.33 M (NH<sub>4</sub>)<sub>2</sub>SO<sub>4</sub> and 0.1 M 2-(N-cyclohexylamino)ethane sulfonic acid (CHES), pH 9.4–9.5. Crystals formed in space group C2, with two molecules per crystallographic asymmetric unit. The crystallization condition for the RZ<sub>1</sub>–Ubc13 complex in both the P1 and the C2 space groups was 8% (w/v) PEG 4000. The P1 and C2 crystals contain one and two complexes per crystallographic asymmetric unit, respectively (Table 1). We collected all diffraction data at beamline X4A of Brookhaven National Laboratory and processed them using HKL2000 (ref. 45).

We determined the RZ<sub>123</sub> structure by SAD<sup>46</sup> from the intrinsic zinc atoms using the programs SOLVE and RESOLVE<sup>47</sup>. We performed iterative model building in WinCoot<sup>48</sup> and refinement in CNS 1.2 (ref. 49). We used molecular replacement to solve the RZ<sub>1</sub>–Ubc13 structure using the CCP4 suite<sup>50</sup>. We generated all structural presentations using PyMOL (DeLano Scientific) and Setor<sup>51</sup>. The final atomic models of RZ<sub>123</sub> in the C2 space group and RZ<sub>1</sub>–Ubc13 in the P1 and C2 space groups contain 86.8%, 83.5% and 79.2% of residues, respectively, in the most favored regions and 100%, 100% and 99.5% of residues, respectively, in the allowed regions of the Ramachandran plots.

**Ubiquitination assays.** We incubated 100 nM mouse E1, 200 nM E2, 2  $\mu$ M wild-type or mutant RZ<sub>123</sub>, RZ<sub>1</sub> or RZ<sub>1234</sub> and 20  $\mu$ M ubiquitin at 37 °C for 45 min in reaction buffer containing 25 mM Tris-HCl, pH 7.5, 2.5 mM MgCl<sub>2</sub>, 0.1 mM DTT, 2 mM ATP, 5 mM creatine phosphate, 0.6 units ml<sup>-1</sup> creatine kinase and 0.6 units ml<sup>-1</sup> inorganic pyrophosphatase. We quenched the reactions using SDS loading buffer and resolved them on 15% (v/v) SDS-PAGE. We transferred the protein bands to PVDF membranes using a Tran-Blot SD Semi-Dry Transfer Cell (BioRad). We probed the membranes with anti-ubiquitin primary antibody (Santa Cruz Biotechnology) in a 1:1,000 dilution, washed them and then incubated them with horseradish peroxidase (HRP)-linked anti-mouse secondary IgG (Cell Signaling) in a 1:4,000 dilution. We used the SuperSignal West Pico Trial Kit (Pierce) to visualize the reactive bands as instructed by the manufacturer.

**Surface plasmon resonance.** We assayed the interaction between TRAF6 RZ<sub>123</sub> and Ubc13 at 25 °C using a Biacore 2000 optical biosensor equipped with a CM4 sensor chip and equilibrated with 20 mM Tris-HCl, pH 7.5, 100 mM NaCl, 5 mM DTT, 0.005% (v/v) Tween-20 and 0.1 mg ml<sup>-1</sup> BSA. We immobilized TRAF6 RZ<sub>123</sub> using amine-coupling chemistry to sensor chips

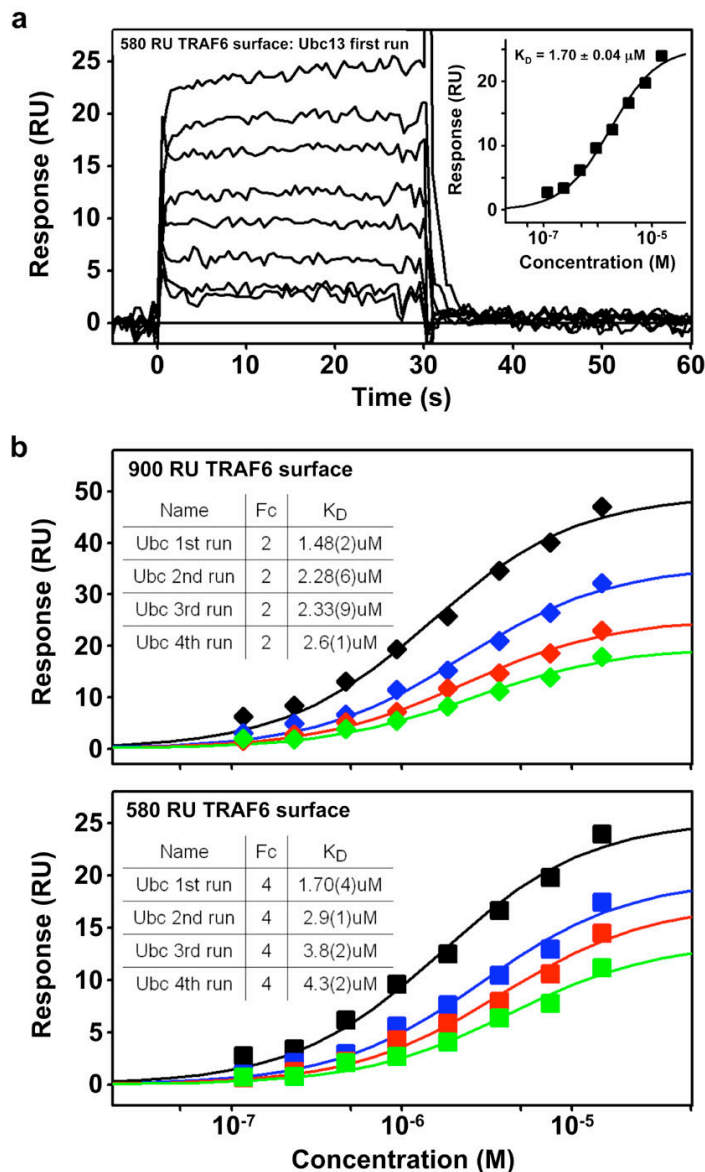
at 580 response units (RU) and 900 RU, respectively, in running buffer containing 20 mM Tris-HCl, pH 7.5, 100 mM NaCl and 5 mM DTT. We tested binding of Ubc13 to the surface-tethered TRAF6 in two-fold dilution series of 0.12, 0.23, 0.47, 0.94, 1.88, 3.75, 7.5 and 15.0  $\mu$ M. We double referenced the binding responses<sup>52</sup> and fit them to a simple binding isotherm to determine the affinities using the program Scrubber 2 (BioLogic Software).

**Small-angle X-ray scattering.** We collected SAXS data at the SIBYLS beamline (12.3.1) at the Advanced Light Source at Lawrence Berkeley National Laboratory. The incident wavelength used in the experiment was 1.54 Å with a  $q$  range of 0.011–0.21 Å<sup>-1</sup> ( $q = 4\pi \sin(\theta/2)/\lambda$ , where  $\theta$  is the scattering angle and  $\lambda$  is the wavelength). The detector was a MAR 165 CCD area detector. We used a 1-mm cuvette with sample volumes of 15  $\mu$ l. We collected data sets at concentrations of approximately 10 mg ml<sup>-1</sup> for both the wild type and the F118A mutant and processed them similarly, as described<sup>53</sup>. Briefly, we used a Guinier plot from scattering curves extrapolated to zero concentration to determine the radius of gyration  $R_g$  (Guinier) using the freeware program PRIMUS<sup>54</sup>. We subjected the scattering curves to an indirect Fourier transform using the GNOM program<sup>55</sup> to yield the pair distribution function  $P(r)$ , from which we derived the maximum dimension and the radius of gyration  $R_g$  ( $P(r)$ )<sup>56</sup>. We also generated the low-resolution *ab initio* model from the values of GNOM output using the dummy atom approach as implemented in GASBOR<sup>57</sup>. Ten runs of GASBOR with and without two-fold symmetry yielded similar results. Results from each independent run agreed well with one another, as judged by the program DAMAVER<sup>58</sup>. We calculated the scattering profiles from PDB files using the program CRY SOL<sup>33</sup> with an option that best fits the data by adjusting properties of the hydration shell. We used the algorithm for elongated proteins to extract the radius of gyration of cross-section ( $R_{xc}$ )<sup>59</sup>.

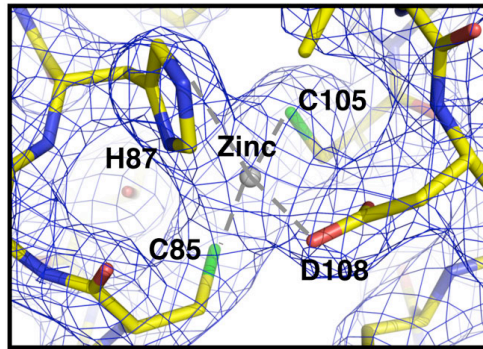
45. Otwinowski, Z. & Minor, W. Processing of X-ray diffraction data collected in oscillation mode. *Methods Enzymol.* **276**, 307–326 (1997).
46. Hendrickson, W.A. Analysis of protein structures from diffraction measurements at multiple wavelengths. *Trans. Am. Crystallogr. Assoc.* **21**, 11 (1985).
47. Terwilliger, T. SOLVE and RESOLVE: automated structure solution, density modification and model building. *J. Synchrotron Radiat.* **11**, 49–52 (2004).
48. Emsley, P. & Cowtan, K. Coot: model-building tools for molecular graphics. *Acta Crystallogr. D Biol. Crystallogr.* **60**, 2126–2132 (2004).
49. Brunger, A.T. *et al.* Crystallography & NMR system: a new software suite for macromolecular structure determination. *Acta Crystallogr. D Biol. Crystallogr.* **54**, 905–921 (1998).
50. Collaborative Computational Project N. The CCP4 suite: programs for protein crystallography. *Acta Crystallogr. D Biol. Crystallogr.* **50**, 760–763 (1994).
51. Evans, S.V. SETOR: hardware-lighted three-dimensional solid model representations of macromolecules. *J. Mol. Graph.* **11**, 134–138 (1993).
52. Myszkka, D.G. Improving biosensor analysis. *J. Mol. Recognit.* **12**, 279–284 (1999).
53. Iyer, R.R. *et al.* The MutS $\alpha$ -proliferating cell nuclear antigen interaction in human DNA mismatch repair. *J. Biol. Chem.* **283**, 13310–13319 (2008).
54. Konarev, P.V., Volkov, V.V., Sokolova, A.V., Koch, M.H.J. & Svergun, D.I. PRIMUS: a Windows PC-based system for small-angle scattering data analysis. *J. Appl. Crystallogr.* **36**, 1277–1282 (2003).
55. Svergun, D.I. Determination of the regularization parameter in indirect-transform methods using perceptual criteria. *J. Appl. Crystallogr.* **25**, 495–503 (1992).
56. Nagar, B. *et al.* Organization of the SH3–SH2 unit in active and inactive forms of the c-Abl tyrosine kinase. *Mol. Cell* **21**, 787–798 (2006).
57. Svergun, D.I., Petoukhov, M.V. & Koch, M.H. Determination of domain structure of proteins from X-ray solution scattering. *Biophys. J.* **80**, 2946–2953 (2001).
58. Kozin, M.B. & Svergun, D.I. Automated matching of high- and low-resolution structural models. *J. Appl. Crystallogr.* **34**, 33–41 (2001).
59. Glatter, O. & Kratky, O. *Small Angle X-ray Scattering* (Academic, London, 1982).

## E2 interaction and dimerization in the crystal structure of TRAF6

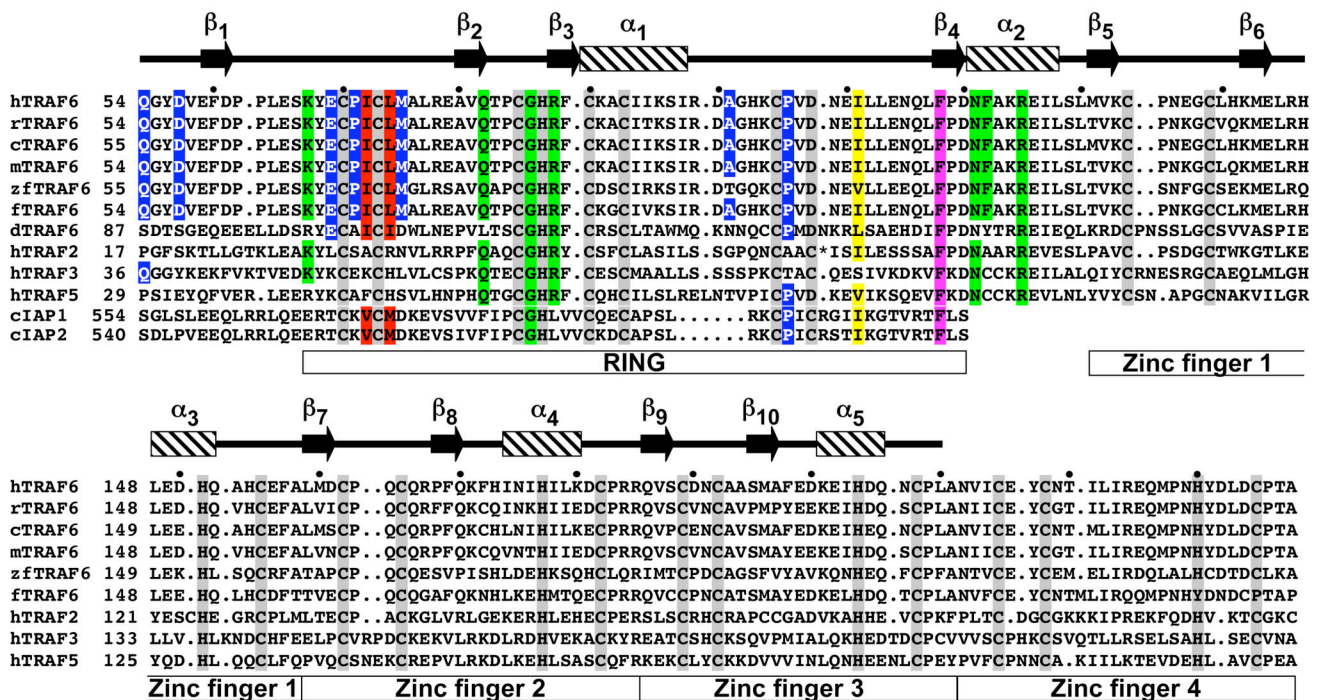
Qian Yin, Su-Chang Lin, Betty Lamothe, Miao Lu, Yu-Chih Lo, Gregory Hura, Lixin Zheng, Rebecca L. Rich, Alejandro D. Campos, David G. Myszka, Michael J. Lenardo, Bryant G. Darnay and Hao Wu



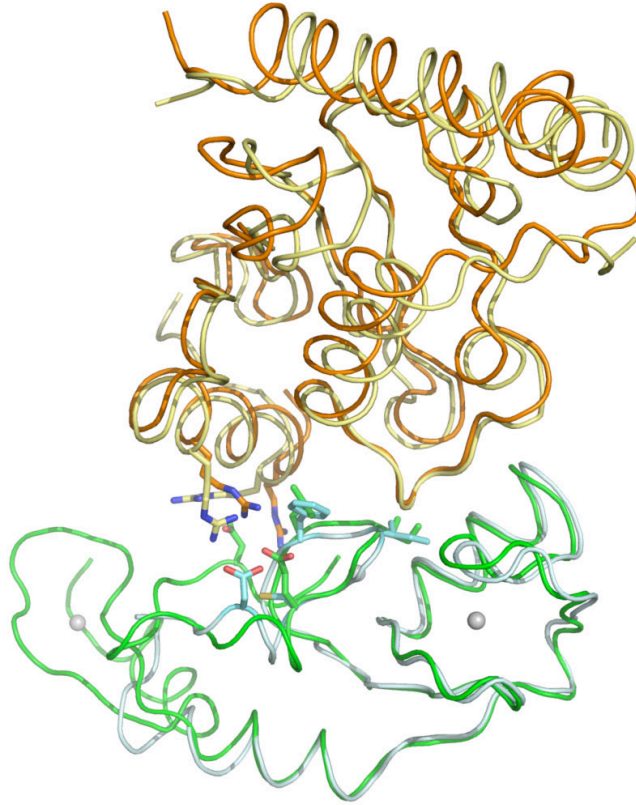
**Supplementary Figure 1.** Quantitative measurement on the interaction between TRAF6 and Ubc13 using SPR. **(a)** Binding of Ubc13 at a series of concentrations to the 580 RU surface coupled with TRAF6 RZ<sub>123</sub>. The responses at 10-20 seconds were plotted against Ubc13 concentration and fit to a simple binding isotherm to obtain affinity information. **(b)** To establish the reproducibility of the SPR measurements, the experiment was repeated another three times at both 900 and 580 RU surfaces, which showed a gradual loss in response intensity over time. The decay in intensity indicates that the TRAF6 surfaces were losing appreciable activity during the time required for these measurements. Black: first run; blue: second run; red: third run; green: fourth run. The fitted dissociation constants were shown.



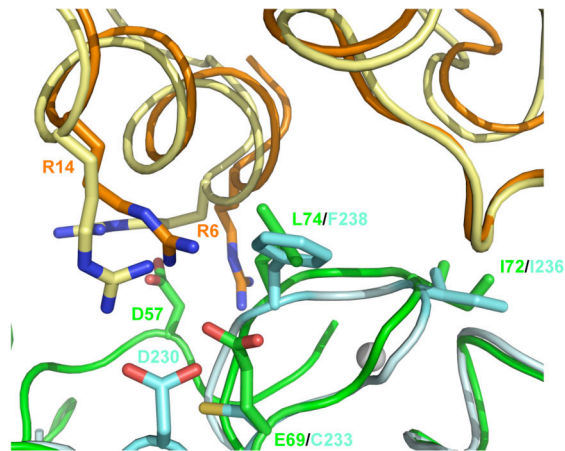
**Supplementary Figure 2.** 2Fo-Fc Electron density map (contoured at 1.0  $\sigma$ ) at one of the zinc coordinating regions of the TRAF6 RZ<sub>123</sub> structure



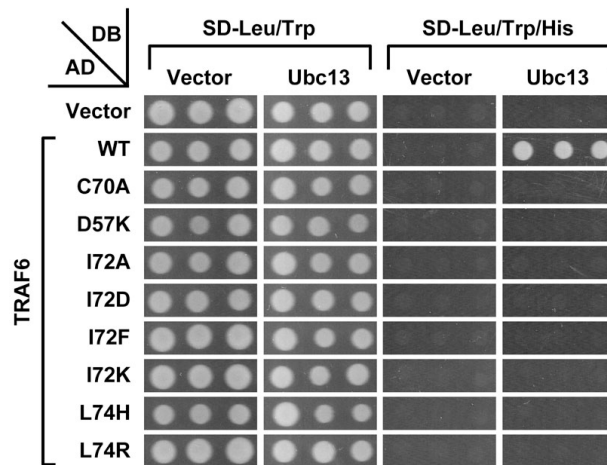
**Supplementary Figure 3.** Sequence alignment of TRAF6 from different species and with TRAF2, TRAF3, TRAF5, cIAP1 and cIAP2. Domain boundaries and secondary structures are labeled. Zinc-coordinating residues in the RING and zinc fingers 1-4 domains are shaded in gray. Residues at the Ubic13 interface are highlighted in red for those that bury more than 60  $\text{\AA}^2$  surface area and in blue for those with surface area burials of 20-60  $\text{\AA}^2$ . Residues at the dimerization interface are highlighted in magenta for those that bury more than 100  $\text{\AA}^2$  surface area and in green for those with surface area burials of 40-100  $\text{\AA}^2$ . The conserved residue at the modeled tetramerization interface is highlighted in yellow. "\*" in the TRAF2 sequence represents an insertion of "VHEGIYEEG". h: human; r: rat; c: cow; m: mouse; zf: zebra fish; f: fowl; d: drosophila.



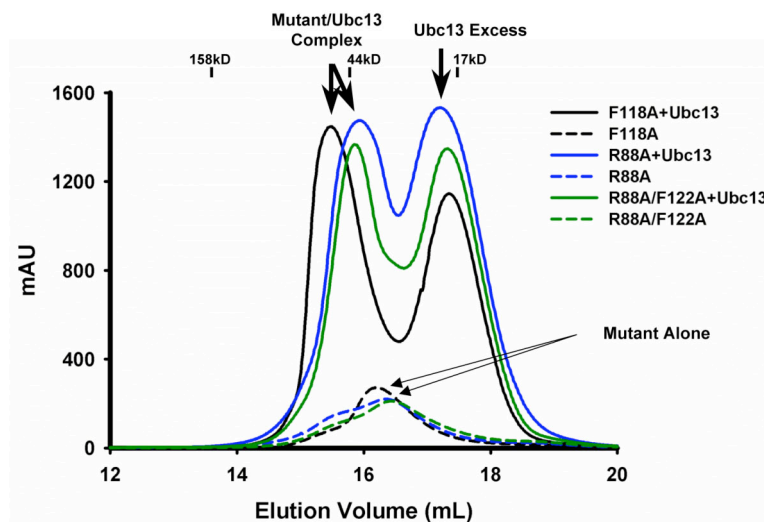
**Supplementary Figure 4.** Superposition of the TRAF6/Ubc13 complex with the CHIP/Ubc13 complex. Green: TRAF6; Cyan: CHIP; orange: Ubc13 in the TRAF6 complex; yellow: Ubc13 in the CHIP complex.



**Supplementary Figure 5.** Details in the superposition of the TRAF6/Ubc13 complex with the CHIP/Ubc13 complex. Green: TRAF6; Cyan: CHIP; orange: Ubc13 in the TRAF6 complex; yellow: Ubc13 in the CHIP complex.



**Supplementary Figure 6.** Yeast two hybrid experiments of Ubc13 binding mutants of full-length TRAF6. C70 is a zinc-coordinating residue in TRAF6 RING and C70A is a negative control for Ubc13 interaction.



**Supplementary Figure 7.** The dimerization mutants of TRAF6 RZ<sub>123</sub> F118A, R88A and R88A/F122A retained their interactions with Ubc13 on gel filtration chromatography. Approximate elution positions of molecular weight standards are shown.

## Supplementary Methods

**Yeast two-hybrid analysis.** We received the *S. cerevisiae* strain AH109 as a generous gift from Dr. Shrikanth Reddy (UTMDACC). We co-transformed yeast cells with the indicated genes in pGAD-T7 and pGBK-T7 based plasmids using the lithium acetate method as stated by the manufacturer (Clontech). Following double selection on synthetic-dextrose (SD) lacking Trp and Leu (SD-Trp-Leu), we picked at least three separate colonies and spotted them onto both SD-Trp-Leu and SD-Trp-Leu-His (with 5 mM 1,2,4-amino triazole) plates. We incubated the plates at 30 °C until growth appeared on the master plate (SD-Trp-Leu), typically within 2-3 days, and determined positive interactions as equivalent growth of colonies on SD-Trp-Leu-His plates.

**Transfection, reporter gene assays, and retroviral infection.** We Transfected HEK293 cells, produced retroviral supernatants and performed retroviral infection essentially as described previously<sup>1,2</sup>.

**Immunoprecipitation, western blotting and in vitro kinase assay.** We left the cells unstimulated or stimulated as indicated in the figure legends and washed them twice with PBS. Depending on the experiment, we lysed the cells with lysis buffer and processed them for immunoprecipitation, western blotting, and in vitro kinase assay as previously described<sup>1,2</sup>.

**FRET assay.** We fused wild type or F118A mutant mouse TRAF6-coding sequences at the N-terminus of Cerulean or Venus coding sequences. We transiently transfected the expression constructs into BJAB lymphoma cells by electroporation, in which we re-suspended 4 million cells in 400  $\mu$ l of complete RPMI medium in a 0.4-cm cuvette, with a total of 20  $\mu$ g DNA. We electroporated the cells at 260 V, 1050 mF, and 720 W, using a BTX-600 machine. We cultured the cells for 24~36 hours before analyzing them using flow-cytometry with A BD LSR II system. We examined fusion-protein expression using excitation lasers of 407 nm /488 nm and measuring emissions at 470 nm /550 nm for Cerulean and Venus respectively. We detected FRET at a 550 /50 nm band-pass filter by excitation at 407nm.

**Confocal microscopy of TRAF6 distribution.** We incubated BJAB cells (ATCC) with 10  $\mu$ g ml<sup>-1</sup> of lipopolysaccharides (LPS) (Sigma) for 2 hours and subjected them to the following processes at room temperature. We washed the cells with PBS twice, re-suspended them in 1 ml of 1 % (v/v) paraformaldehyde/PBS for 15 minutes, and washed them once with PBS. We used Cytospin to transfer the fixed cells onto poly lysine-coated microscope slides. We permeabilized the mounted cells with 0.2 % (v/v) Triton X-100/PBS for 30 minutes, blocked them by 1 % (w/v) BSA in PBS for 1 hour, and stained them with 1  $\mu$ g ml<sup>-1</sup> of rabbit anti-TRAF6 (ZyMED) for 1 hour. We washed the cells 3 times with PBS and stained them with Alexa Fluor 568-goat-anti-rabbit IgG (Molecular Probes) (1:500) and 1  $\mu$ M Hoechst 33342 (Molecular Probes) for 1 hour. We then rinsed the slides 3 times against PBS and mounted them with cover slides. We used a Leica Sp1 confocal microscope to scan images of TRAF6 and nucleus staining and the Imaris 6.1 software to analyze at least 10 40-x-images for each treatment.

1. Lamothe, B. et al. Site-specific Lys-63-linked tumor necrosis factor receptor-associated factor 6 auto-ubiquitination is a critical determinant of I kappa B kinase activation. *J Biol Chem* **282**, 4102-12 (2007).
2. Besse, A. et al. TAK1-dependent signaling requires functional interaction with TAB2/TAB3. *J Biol Chem* **282**, 3918-28 (2007).